Transmon probe for quantum characteristics of magnons in antiferromagnets

Vahid Azimi-Mousolou [1,2,*] Anders Bergman,[2] Anna Delin,[3,4] Olle Eriksson,[2] Manuel Pereiro,[2]
Danny Thonig,[5] and Erik Sjöqvist [2,†]

[1]*Department of Applied Mathematics and Computer Science, Faculty of Mathematics and Statistics, University of Isfahan,
Isfahan 81746-73441, Iran*
[2]*Department of Physics and Astronomy, Uppsala University, Box 516, SE-751 20 Uppsala, Sweden*
[3]*Department of Applied Physics, School of Engineering Sciences, KTH Royal Institute of Technology, AlbaNova University Center,
SE-10691 Stockholm, Sweden*
[4]*Swedish e-Science Research Center (SeRC), KTH Royal Institute of Technology, SE-10044 Stockholm, Sweden*
[5]*School of Science and Technology, Örebro University, SE-701 82 Örebro, Sweden*

The detection of magnons and their quantum properties, especially in antiferromagnetic (AFM) materials, is a substantial step to realize many ambitious advances in the study of nanomagnetism and the development of energy efficient quantum technologies. The recent development of hybrid systems based on superconducting circuits provides the possibility to engineer quantum sensors that exploit different degrees of freedom. Here, we examine the magnon-photon-transmon hybridization based on bipartite AFM materials, which gives rise to an effective coupling between a transmon qubit and magnons in a bipartite AFM. We demonstrate how magnon modes, their chiralities, and quantum properties, such as nonlocality and two-mode magnon entanglement in bipartite AFMs, can be characterized through the Rabi frequency of the superconducting transmon qubit.

I. INTRODUCTION

During the last decade, there have been considerable advancements in the use of magnons for storing, transmitting, and processing information. This rapid progress has turned the emerging research field of magnonics into a promising candidate for innovating information processing technologies [1]. The combination of magnonics with quantum information processing provides a highly interdisciplinary physical platform for the study of various quantum phenomena in spintronics, quantum electrodynamics, and quantum information science. Indeed, the quantum magnonics exhibits distinct quantum properties, which can be utilized for multipurpose quantum tasks [2–6].

Despite significant progress in quantum magnonics [2–25], there are still many features and challenges that need to be addressed in theory and in the laboratory. In particular, the experimental verification of nonclassical magnon states and quantum properties such as squeezed and entangled states would pave the way for many possible research strategies. The key point is interconnections between magnetic materials

and electronic quantum systems. Superconducting qubits have been successfully used to detect magnons in ferromagnetic materials [7]. However, antiferromagnetic (AFM) materials are more sustainable for quantum applications as they offer lower magnetic susceptibility, faster dynamics, smaller device features, and lower energy consumption compared to ferromagnetic materials [1]. Recently, we have theoretically examined magnon-magnon entanglement and squeezing in AFMs [21–23].

Here, we examine the possibility to combine the advantageous features of transmon and AFM materials. To this end, we demonstrate effective coupling between a superconducting transmon qubit and a bipartite AFM material. We show how the polarized (chiral) magnons and bipartite magnon-magnon entanglement in the AFM can be detected through the measurement of Rabi frequency of the transmon qubit. The proposed setup is suitable for the experimental study of the quantum properties of magnons in a wide range of crystalline and synthetic AFM materials, such as NiO and MnO, MnF_2 and FeF_2, two-dimensional Ising systems such as $MnPSe_3$, YIG-based synthetic AFMs, and perovskite manganites [13,26–33]. The present work differs from existing studies on ferromagnetic-based hybrid magnonic systems [5–12]. This is because the hybrid magnonics discussed here is based on magnons in AFM materials, which are conceptually distinct from magnons in ferromagnetic materials. Unlike in ferromagnets, magnons in AFMs appear in twin pairs with opposite chiralities [1,34–36]. Therefore, a polarized chiral photon [37] is required to achieve the appropriate hybridization, as demonstrated below. In addition, our research seeks to characterize magnon chirality and magnon entanglement

*v.azimi@sci.ui.ac.ir
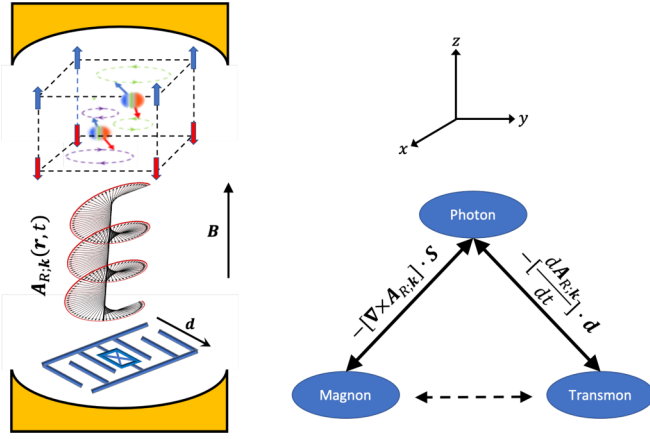†erik.sjoqvist@physics.uu.se

FIG. 1. Schematic illustration of magnon-photon-transmon hybridization. A circularly polarized microwave cavity electromagnetic field, which is described by the vector potential $\mathbf{A}_{R;\mathbf{k}}(\mathbf{r}, t)$, can interact with magnons in an antiferromagnetic material and a superconducting transmon qubit. The cavity walls are illustrated with yellow segments in the left panel. An antiferromagnetic material hosts two chiral magnons, which are shown with three-color balls in the cubic lattice inside the cavity. Two magnons are degenerate in the absence of magnetic field and a small external magnetic field $\mathbf{B}$ in the z direction breaks this degeneracy (see, also, Fig. 2). While the coupling between the magnon and cavity field is achieved through magnetic-dipole interaction, an electric-dipole interaction describes the coupling between the cavity field and transmon (right panel).

using superconducting qubits, which has not been explored in prior works such as Refs. [5–12].

The outline of the paper is as follows. In Sec. II, we describe magnon-photon-transmon hybridization and derive the interacting Hamiltonian. In Sec. III, we discuss two-mode magnon entanglement in AFM materials. In Sec. IV, we obtain an effective magnon-transmon coupling and show how this effective coupling mechanism allows one to experimentally study quantum characteristics of magnons in antiferromagnetic materials. The paper ends with a conclusion in Sec. V.

II. MAGNON-PHOTON-TRANSMON HYBRIDIZATION

In this section, we describe a photon-mediated coupling mechanism between a superconducting transmon qubit and polarized magnons in a bipartite AFM. We assume a hybrid system composed of a single crystal or synthetic AFM, a transmon-type superconducting qubit, and a microwave cavity, as illustrated in Fig. 1. The system hosts four modes, including two magnon modes in an AFM compound, a transmon qubit, and a microwave cavity electromagnetic mode. The dynamics of the hybridized magnon-photon-transmon system can be described by the Hamiltonian

$$H = H_{\text{m}} + H_{\text{ph}} + H_{\text{m-ph}} + H_{\text{q}} + H_{\text{ph-q}}, \quad (1)$$

where the term H_{m} describes the magnon subsystem, H_{ph} describes the microwave photon, $H_{\text{m-ph}}$ describes the magnon-photon interaction, H_{q} describes the transmon, and $H_{\text{ph-q}}$ describes the photon-transmon interaction. They are described in detail as follows.
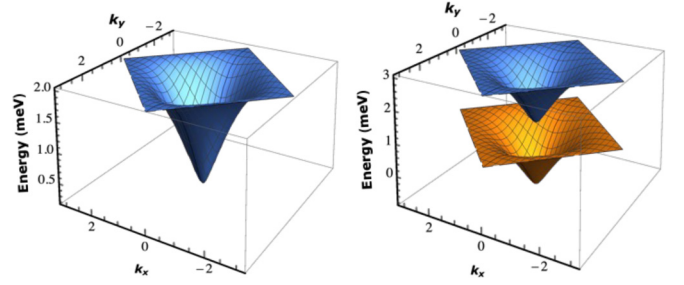

FIG. 2. Magnon energy dispersions $\omega_{\alpha_{\mathbf{k}}}$ and $\omega_{\beta_{-\mathbf{k}}}$ in the first Brillouin zone of a square lattice with lattice constant $a = 1$ for an easy-axis AFM. As model parameters, we use $|J| = 1$ meV for antiferromagnetic Heisenberg exchange, $\mathcal{K}_z = 0.01J$ for uniaxial anisotropy, and $S = 1/2$. Two magnons are degenerate in the absence of an external magnetic field $\mu_B B = 0$ (left panel). A magnetic field $\mu_B B = 1$ meV in the z direction breaks the degeneracy (right panel).

Two-mode magnon system. H_{m} represents a two-mode magnon Hamiltonian in a bipartite treatment of an AFM material. Consider an AFM spin Hamiltonian $H_{\text{s}} = \sum_{i,j} \mathbf{S}_i \mathbb{I}_{ij} \mathbf{S}_j + \sum_i \mathbf{B} \cdot \mathbf{S}_i$, where $\mathbf{S}_i$ is the spin vector operator at lattice site i, $\mathbb{I}_{ij}$ is the bilinear interaction tensor matrix between sites i and j, and $\mathbf{B}$ is an external field. By applying the Holstein-Primakoff transformation at low temperature followed by the Fourier transformation to the AFM spin Hamiltonian, H_{m} can be described in terms of a pair of interacting collective bosonic modes in the lattice momentum $\mathbf{k}$ space as [21,22] (we assume $\hbar = 1$ throughout the paper)

$$
\begin{aligned}
H_{\text{m}}^{\mathbf{k}} = {} & \omega_{a_{\mathbf{k}}} a_{\mathbf{k}}^{\dagger} a_{\mathbf{k}} + \omega_{b_{-\mathbf{k}}} b_{-\mathbf{k}}^{\dagger} b_{-\mathbf{k}} \\
& + g_{\text{m-m}}^{\mathbf{k}} a_{\mathbf{k}} b_{-\mathbf{k}} + \left(g_{\text{m-m}}^{\mathbf{k}}\right)^* a_{\mathbf{k}}^{\dagger} b_{-\mathbf{k}}^{\dagger}.
\end{aligned}
\quad (2)
$$

The $a_{\mathbf{k}}^{\dagger}$ ($a_{\mathbf{k}}$) and $b_{-\mathbf{k}}^{\dagger}$ ($b_{-\mathbf{k}}$) are bosonic creation (annihilation) operators on the two sublattices A and B with opposite magnetizations in the bipartite AFM. Bosonic operators on opposite sublattices commute and define a pair of interacting magnons in the Kittel (a, b) modes. The Kittel modes can be hybridized into the diagonal magnon modes (α, β) through the SU(1,1) Bogoliubov transformation,

$$
\begin{pmatrix} a_{\mathbf{k}} \\ b_{-\mathbf{k}}^{\dagger} \end{pmatrix} = \begin{pmatrix} u_{\mathbf{k}} & v_{\mathbf{k}} \\ v_{\mathbf{k}}^* & u_{\mathbf{k}}^* \end{pmatrix} \begin{pmatrix} \alpha_{\mathbf{k}} \\ \beta_{-\mathbf{k}}^{\dagger} \end{pmatrix}, \quad (3)
$$

where $u_{\mathbf{k}} = \cosh(r_{\mathbf{k}})$ and $v_{\mathbf{k}} = \sinh(r_{\mathbf{k}})e^{i\phi_{\mathbf{k}}}$, with

$$r_{\mathbf{k}} = \tanh^{-1}\left[\frac{1 - \sqrt{1 - |\Gamma_{\mathbf{k}}|^2}}{|\Gamma_{\mathbf{k}}|}\right] \geqslant 0,$$

$$\phi_{\mathbf{k}} = \pi - \arg[\Gamma_{\mathbf{k}}], \quad \Gamma_{\mathbf{k}} = \frac{2g_{\text{m-m}}^{\mathbf{k}}}{\omega_{a_{\mathbf{k}}} + \omega_{b_{-\mathbf{k}}}}. \quad (4)$$

In terms of the (α, β) modes, the magnon Hamiltonian $H_{\text{m}}^{\mathbf{k}}$ takes the diagonal form,

$$H_{\text{m}}^{\mathbf{k}} = \omega_{\alpha_{\mathbf{k}}} \alpha_{\mathbf{k}}^{\dagger} \alpha_{\mathbf{k}} + \omega_{\beta_{-\mathbf{k}}} \beta_{-\mathbf{k}}^{\dagger} \beta_{-\mathbf{k}}. \quad (5)$$

The bosonic diagonal modes labeled as α and β describe right and left circularly polarized (chiral) magnons [1,34–36]. As illustrated in Fig. 2, for an easy-axis AFM in the absence of an external magnetic field [$H_{\text{s}} = J \sum_{i,j} \mathbf{S}i \cdot \mathbf{S}j + \mathcal{K}z \sum i (S^z i)^2$], the two magnon modes are degenerate,

meaning $\omega_{\alpha_{\mathbf{k}}} = \omega_{\beta_{-\mathbf{k}}} = \omega_{\mathbf{k}}$. However, introducing a magnetic field in the z direction, denoted as $H_s + B \sum_i S_i^z$, breaks this degeneracy, resulting in $\omega_{\alpha_{\mathbf{k}}} = \omega_{\mathbf{k}} - B$ and $\omega_{\beta_{-\mathbf{k}}} = \omega_{\mathbf{k}} + B$ [21,22].

Microwave photon. For the second term of the hybrid Hamiltonian in Eq. (1), we assume a right circularly polarized microwave cavity electromagnetic field with the single cavity mode frequency $\omega_{c_{\mathbf{k}}}$ [20,22,24,36]. This is described by the vector potential

$$\mathbf{A}_{R;\mathbf{k}}(\mathbf{r}, t) = A_0 \big[\mathbf{e}_R c_{\mathbf{k}} e^{-i(\mathbf{k}\cdot\mathbf{r}+\omega_{c_{\mathbf{k}}}t)} + \mathbf{e}_R^* c_{\mathbf{k}}^\dagger e^{i(\mathbf{k}\cdot\mathbf{r}+\omega_{c_{\mathbf{k}}}t)} \big]$$
$$= e^{it\omega_{c_{\mathbf{k}}} c_{\mathbf{k}}^\dagger c_{\mathbf{k}}} \mathbf{A}_{R;\mathbf{k}}(\mathbf{r}, 0) e^{-it\omega_{c_{\mathbf{k}}} c_{\mathbf{k}}^\dagger c_{\mathbf{k}}}. \quad (6)$$

The vector $\mathbf{k}$ is the propagation direction of the electromagnetic wave, A_0 is the amplitude of the vector potential, and $c_{\mathbf{k}}(c_{\mathbf{k}}^\dagger)$ is the annihilation (creation) operator of the right circularly polarized photon with unit vector $\mathbf{e}_R = \frac{1}{\sqrt{2}}(1, -i, 0)$. Both $\omega_{c_{\mathbf{k}}}$ and A_0 can be tuned by changing the volume of the cavity and the separation distance between the two conductor plates in the cavity. Here, we focus on the lowest-energy cavity mode and disregard contributions from the higher-energy cavity modes. In the rotating frame, the photon contribution to the full Hamiltonian in Eq. (1) is

$$H_{\text{ph}}^{\mathbf{k}} = \omega_{c_{\mathbf{k}}} c_{\mathbf{k}}^\dagger c_{\mathbf{k}}, \quad (7)$$

for a given $\mathbf{k}$.

Magnon-photon interaction. By turning on the electromagnetic field, the magnon modes start to interact with the cavity mode through the magnetic-dipole coupling. Explicitly, the electromagnetic field induces a magnetic field $\mathbf{B}_{\text{ph}}$, which interacts with the total spin $\mathbf{S}$ of the AFM material through the Zeeman interaction term [20,22,24,36],

$$H_{\text{m-ph}} = -\mathbf{B}_{\text{ph}} \cdot \mathbf{S}. \quad (8)$$

In the rotating frame, the photon-induced magnetic field is given by $\mathbf{B}_{\text{ph}} = \nabla \times \mathbf{A}_{\mathbf{k}}(\mathbf{r}, 0)$. Following the bosonization procedure used to derive the Hamiltonian $H_m^{\mathbf{k}}$, we obtain the bosonized resonant magnon-photon interaction Hamiltonian,

$$H_{\text{m-ph}}^{\mathbf{k}} = -g_{\text{m-ph}}^{\mathbf{k}} c_{\mathbf{k}}^\dagger \alpha_{\mathbf{k}} + \text{H.c.} \quad (9)$$

The off-resonant interaction $(-g_{\text{m-ph}}^{\mathbf{k}} c_{\mathbf{k}} \beta_{-\mathbf{k}} + \text{H.c.})$ is neglected due to energy conservation. Here, the magnon-photon exchange coupling is

$$g_{\text{m-ph}}^{\mathbf{k}} = \lambda_{\mathbf{k}}(u_{\mathbf{k}} + v_{\mathbf{k}}^*), \quad (10)$$

with $\lambda_{\mathbf{k}} = A_0 k \sqrt{S}$, and we choose to study the case when $\mathbf{k} = (0, 0, k)$.

Transmon qubit. The third subsystem consists of a superconducting qubit described by the Hamiltonian [38]

$$H_q = 4E_C \hat{n}^2 - E_J \cos \hat{\phi}, \quad (11)$$

where the first term corresponds to the kinetic energy contribution from a capacitor and the second term is the potential energy contribution by a Josephson junction. At a sufficiently large E_J/E_C, the superconducting system enters the transmon qubit regime. Following the ladder operator approach, one may represent the momentum $\hat{n}$ and position $\hat{\phi}$ operators in

terms of bosonic annihilation (creation) operator η ($\eta^\dagger$) as

$$\hat{n} = i \left(\frac{E_J}{32E_C} \right)^{1/4} (\eta^\dagger - \eta),$$
$$\hat{\phi} = \left(\frac{2E_C}{E_J} \right)^{1/4} (\eta^\dagger + \eta). \quad (12)$$

By using the ladder representation, one can write the Hamiltonian in Eq. (11) in the form of the following anharmonic oscillator Hamiltonian:

$$H_q \approx \left[\omega_q + \frac{\xi}{2} \right] \eta^\dagger \eta - \frac{\xi}{2} (\eta^\dagger \eta)^2. \quad (13)$$

This follows from a Taylor expansion of the potential energy term in Eq. (11) and a rotating wave approximation. Here, $\omega_q = \sqrt{8E_C E_J} - E_C$ defines the Rabi transition frequency between the ground state $|g\rangle$ and the first excited state $|e\rangle$, and $\xi = E_C$ is the anharmonicity. In the transmon regime, the anharmonicity is negative and large enough that allows one to focus on the two lowest-energy levels of the anharmonic oscillator as a transmon qubit, the Hamiltonian of which can be conveniently reduced to

$$H_q = \omega_q \eta^\dagger \eta. \quad (14)$$

Photon-transmon interaction. The large electric dipole of the superconducting qubit, $\hat{\mathbf{d}} = \mathbf{d}\eta^\dagger + \mathbf{d}^*\eta$, can strongly couple to the induced electric field of the microwave photon through electric-dipole coupling [38],

$$H_{\text{ph-q}} = -\mathbf{E}_{\text{ph}} \cdot \hat{\mathbf{d}}, \quad (15)$$

where $\mathbf{E}_{\text{ph}} = \frac{d\mathbf{A}_{\mathbf{k}}(\mathbf{r},t)}{dt}$ determines the photon-induced electric field. If we assume $\mathbf{d}||\mathbf{e}_R$, then, under the rotating wave approximation, the photon-qubit interaction is described by the Hamiltonian

$$H_{\text{ph-q}}^{\mathbf{k}} = -g_{\text{ph-q}}^{\mathbf{k}} \eta^\dagger c_{\mathbf{k}} + \text{H.c.}, \quad (16)$$

where the photon-qubit exchange coupling is given by

$$g_{\text{ph-q}}^{\mathbf{k}} = -id\omega_{c_{\mathbf{k}}} \exp[-i\mathbf{k} \cdot \mathbf{r}], \quad (17)$$

with $d = |\mathbf{d}|$ being the strength of the electric dipole of the superconducting transmon qubit.

Having specified each term in the Hamiltonian of Eq. (1), we conclude that the magnon-photon-transmon hybrid system is explicitly described by the bosonized Hamiltonian

$$H_{\mathbf{k}} = \omega_{\alpha_{\mathbf{k}}} \alpha_{\mathbf{k}}^\dagger \alpha_{\mathbf{k}} + \omega_{\beta_{-\mathbf{k}}} \beta_{-\mathbf{k}}^\dagger \beta_{-\mathbf{k}} + \omega_{c_{\mathbf{k}}} c_{\mathbf{k}}^\dagger c_{\mathbf{k}} + \omega_q \eta^\dagger \eta$$
$$- \big[g_{\text{m-ph}}^{\mathbf{k}} c_{\mathbf{k}}^\dagger \alpha_{\mathbf{k}} + g_{\text{ph-q}}^{\mathbf{k}} \eta^\dagger c_{\mathbf{k}} + \text{H.c.} \big], \quad (18)$$

for a momentum $\mathbf{k}$ vector in the z direction, with the in-plane parallel photon polarization vector $\mathbf{e}_R$ and the superconducting dipole $\mathbf{d}||\mathbf{e}_R$.

It is important to note that only the hybridized magnon in the α mode couples with the photon and transmon modes in the Hamiltonian in Eq. (18). In other words, the β magnon mode is effectively decoupled from the other modes in the system. This is due to the fact that we use the right circularly polarized microwave cavity electromagnetic field, which only couples to the magnon with the same polarization, i.e., the α mode. However, if we use a left circularly polarized cavity field, it couples the β magnon mode with the photon and
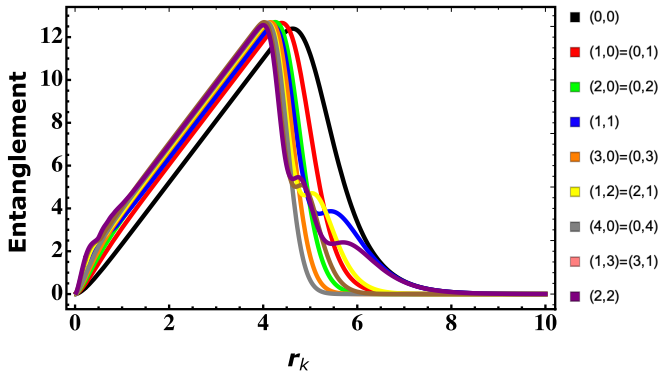
FIG. 3. Entanglement of magnon eigenstates corresponding to pairs of magnon numbers (x, y) against the entanglement (squeezing) parameter $r_{\mathbf{k}}$.
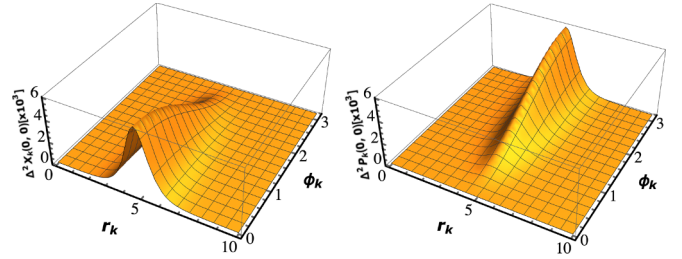

FIG. 4. Vacuum quantum fluctuations of conjugate position, $X_{\mathbf{k}}$, and momentum, $P_{\mathbf{k}}$, quadratures as functions of the parameters $r_{\mathbf{k}}$ and $\phi_{\mathbf{k}}$. The maximum quantum squeezing (stretching) effect is associated with maximum quantum magnon entanglement in the two-mode vacuum ground state shown in Fig. 3. The same effect is observed for all magnon eigenstates associated with any pair of magnon numbers (x, y).

the transmon modes, and instead leaves the α magnon mode decoupled from the rest of the system.

The hybrid quantum system described by Eq. (18) provides a promising platform to observe and verify quantum effects in quantum magnonics and exploit them for new quantum applications. Below we employ this hybrid platform to propose an experimental setup for observing polarized twin magnon modes as well as intrinsic two-mode magnon entanglement in bipartite AFM materials via a transmon qubit. In the next section, we briefly describe the basic concepts of two-mode entanglement in AFMs.

III. MAGNON-MAGNON ENTANGLEMENT

Let us focus on the two-mode magnon Hamiltonian described by $H_{\mathrm{m}}^{\mathbf{k}}$ above. The coupling parameter $g_{\mathrm{m\text{-}m}}^{\mathbf{k}}$ in Eq. (2), which is mainly given by the AFM coupling between the two opposite sublattices A and B, introduces a strong squeezing and entanglement between bosonic magnon modes in a way that all the eigenstates of $H_{\mathrm{m}}^{\mathbf{k}}$ become entangled in the Kittel (a, b) modes [21,22]. Explicitly, the complete energy eigenbasis of the Hamiltonian $H_{\mathrm{m}}^{\mathbf{k}}$ can be expressed in the following form:

$$|\psi_{xy}(r_{\mathbf{k}}, \phi_{\mathbf{k}})\rangle = (\alpha_{\mathbf{k}}^{\dagger})^{x}(\beta_{-\mathbf{k}}^{\dagger})^{y}|\psi_{00}(r_{\mathbf{k}}, \phi_{\mathbf{k}})\rangle, \quad (19)$$

for positive integers x and y, and the two-mode squeezed vacuum ground state,

$$|\psi_{00}(r_{\mathbf{k}}, \phi_{\mathbf{k}})\rangle = \frac{1}{\cosh r_{\mathbf{k}}} \sum_{n=0}^{\infty} e^{in\phi_{\mathbf{k}}} \tanh^{n} r_{\mathbf{k}} |n; a_{\mathbf{k}}\rangle |n; b_{-\mathbf{k}}\rangle, \quad (20)$$

given in the Kittel (a, b) magnon basis. Here, x and y represent the number of magnons in the hybridized magnon modes $\alpha_{\mathbf{k}}$ and $\beta_{-\mathbf{k}}$, respectively. Note that the hybridized magnon modes (α, β) are related to the Kittel magnon modes (a, b) through Eq. (3).

Figure 3 illustrates the entropies of entanglement of the energy eigenbasis in Eq. (19) for selected pairs of magnon numbers (x, y) as functions of the squeezing parameter $r_{\mathbf{k}}$. The squeezing parameter $r_{\mathbf{k}}$, which is given in Eq. (4) by the ratio of the magnon-magnon coupling $g_{\mathrm{m\text{-}m}}^{\mathbf{k}}$ to the average single magnon energies in the Kittel modes, is actually the

only parameter that determines the entropies of entanglement of the complete energy eigenbasis. This follows from the fact that the states in Eq. (19) are determined by $(r_{\mathbf{k}}, \phi_{\mathbf{k}})$ and $\phi_{\mathbf{k}}$ contributes only to the phase factors of the coefficients in the Schmidt decompositions of these states.

Quantum fluctuations (variances) of total position, $X_{\mathbf{k}} = \frac{X_{\mathbf{k}}^{(A)} + X_{\mathbf{k}}^{(B)}}{\sqrt{2}}$, and total momentum, $P_{\mathbf{k}} = \frac{P_{\mathbf{k}}^{(A)} + P_{\mathbf{k}}^{(B)}}{\sqrt{2}}$, quadrature observables (see the Appendix for explicit expressions of quadratures for each sublattices) in the two-mode vacuum ground state are plotted in Fig. 4 as functions of the parameters $r_{\mathbf{k}}$ and $\phi_{\mathbf{k}}$. Comparing to Fig. 3, it is evident that in the case of the two-mode vacuum ground state, the highest degree of quantum magnon entanglement corresponds to the strongest quantum squeezing (or stretching) effect [39,40]. A similar pattern can be observed for all of the other magnon eigenstates associated with a given pair of magnon numbers (x, y).

We remind the reader that the entropy of entanglement for a bipartite state $|\psi\rangle \in H_A \otimes H_B$ is given by

$$E[|\psi\rangle] = -\sum_{n} |\chi_{n}|^{2} \log_{2} |\chi_{n}|^{2}, \quad (21)$$

with χ_{n}'s being the Schmidt coefficients in $|\psi\rangle = \sum_{n} \chi_{n} |i_{n}; A\rangle |j_{n}; B\rangle$, where $|i_{n}; A\rangle$ and $|j_{n}; B\rangle$ are orthonormal states in subsystem A and subsystem B, respectively [41].

For the energy eigenstates in Eq. (19), we obtain the following normalized Schmidt decompositions:

$$|\psi_{xy}(r_{\mathbf{k}}, \phi_{\mathbf{k}})\rangle$$
$$= \begin{cases} \sum_{n=0}^{\infty} p_{n;\mathbf{k}}^{(x,y)} |n + \delta; a_{\mathbf{k}}\rangle |n; b_{-\mathbf{k}}\rangle, & x \geqslant y \\ \sum_{n=0}^{\infty} p_{n;\mathbf{k}}^{(x,y)} |n; a_{\mathbf{k}}\rangle |n + \delta; b_{-\mathbf{k}}\rangle, & x \leqslant y, \end{cases} \quad (22)$$

where $\delta = |x - y|$. Here, the Schmidt coefficients are given by

$$p_{n;\mathbf{k}}^{(x,y)} = \frac{1}{\sqrt{x! y!}} \left(\frac{1}{u_{\mathbf{k}}^{*}}\right)^{\delta} \left(\frac{1}{u_{\mathbf{k}}^{*} v_{\mathbf{k}}}\right)^{m} f_{n;\mathbf{k}}^{(m,\delta)} p_{n;\mathbf{k}}, \quad (23)$$

for $m = \min\{x, y\}$, with

$$p_{n;\mathbf{k}} = \frac{e^{in\phi_{\mathbf{k}}}}{\cosh r_{\mathbf{k}}} \tanh^{n} r_{\mathbf{k}}, \quad (24)$$

and $f_{n;\mathbf{k}}^{(m,\delta)}$ that satisfies the following recursive relations:

$$
\begin{aligned}
f_{n;\mathbf{k}}^{(m,\delta>0)} &= |u_{\mathbf{k}}|^2 \sqrt{n+\delta}\, f_{n;\mathbf{k}}^{(m,\delta-1)} \\
&\quad - |v_{\mathbf{k}}|^2 \sqrt{n+1}\, f_{n+1;\mathbf{k}}^{(m,\delta-1)}, \\
f_{n;\mathbf{k}}^{(m>0,0)} &= n|u_{\mathbf{k}}|^4 f_{n-1;\mathbf{k}}^{(m-1,0)} - (2n+1)|u_{\mathbf{k}}v_{\mathbf{k}}|^2 f_{n;\mathbf{k}}^{(m-1,0)} \\
&\quad + (n+1)|v_{\mathbf{k}}|^4 f_{n+1;\mathbf{k}}^{(m-1,0)},
\end{aligned}
\tag{25}
$$

with $f_{n;\mathbf{k}}^{(0,0)} = 1$ for each n. From Eqs. (23)–(25), it is clear that the absolute value of the Schmidt coefficients $|p_{n;\mathbf{k}}^{(x,y)}|$, and thus the entanglement entropies of all energy eigenbasis states in the Kittel magnon modes (a, b), namely,

$$
E[(\alpha_{\mathbf{k}}^{\dagger})^x (\beta_{-\mathbf{k}}^{\dagger})^y |\psi_{00}\rangle] = -\sum_{n=0}^{\infty} \left| p_{n;\mathbf{k}}^{(x,y)} \right|^2 \log_2 \left| p_{n;\mathbf{k}}^{(x,y)} \right|^2,
\tag{26}
$$

are single variable functions of the squeezing parameter $r_{\mathbf{k}}$. In other words, the squeezing parameter $r_{\mathbf{k}}$ is the only entanglement parameter that determines two-mode magnon entanglement in the AFM system described by $H_{\mathrm{m}}^{\mathbf{k}}$.

In the following, we show how a superconducting transmon qubit can be used to observe different magnons and the squeezing/entanglement parameter $r_{\mathbf{k}}$. The latter allows us to quantify quantum characteristics such as two-mode squeezing and entanglement in AFM materials.

IV. SENSING MAGNONS AND THEIR QUANTUM CHARACTERISTICS WITH TRANSMONS

A. Magnon-transmon effective coupling

The Hamiltonian in Eq. (18), which allows for magnon-photon-transmon hybrid states, provides an effective photon-mediated magnon-transmon coupling. To determine this effective coupling rate, one may use the Schrieffer-Wolff unitary transformation [42],

$$
H_{\mathbf{k}}' = e^{W_{\mathbf{k}}} H_{\mathbf{k}} e^{-W_{\mathbf{k}}},
\tag{27}
$$

to effectively decouple the photon mode from magnon and transmon modes in the hybrid Hamiltonian up to first order.

Consider the following decomposition of the hybrid Hamiltonian in Eq. (18):

$$
\begin{aligned}
H_{\mathbf{k}} &= H_{\mathbf{k};0} + V_{\mathbf{k}}, \\
H_{\mathbf{k};0} &= \omega_{\alpha_{\mathbf{k}}} \alpha_{\mathbf{k}}^{\dagger}\alpha_{\mathbf{k}} + \omega_{c_{\mathbf{k}}} c_{\mathbf{k}}^{\dagger}c_{\mathbf{k}} + \omega_q \eta^{\dagger}\eta, \\
V_{\mathbf{k}} &= -g_{\text{m-ph}}^{\mathbf{k}} c_{\mathbf{k}}^{\dagger}\alpha_{\mathbf{k}} - g_{\text{ph-q}}^{\mathbf{k}} \eta^{\dagger}c_{\mathbf{k}} + \text{H.c.},
\end{aligned}
\tag{28}
$$

where we neglect the magnon β mode as it is decoupled from the rest of the Hamiltonian $H_{\mathbf{k}}$. By using the Baker-Campbell-Haussdorf formula, the transformation in Eq. (27) can be expanded as

$$
\begin{aligned}
H_{\mathbf{k}}' &= H_{\mathbf{k};0} + V_{\mathbf{k}} + [W_{\mathbf{k}}, H_{\mathbf{k};0}] + [W_{\mathbf{k}}, V_{\mathbf{k}}] \\
&\quad + \tfrac{1}{2}[W_{\mathbf{k}}, [W_{\mathbf{k}}, H_{\mathbf{k};0}]] + \tfrac{1}{2}[W_{\mathbf{k}}, [W_{\mathbf{k}}, V_{\mathbf{k}}]] + \cdots.
\end{aligned}
\tag{29}
$$

This three-mode Schrieffer-Wolff Hamiltonian can be made block diagonal, turning the system into a two-mode magnon-transmon subsystem decoupled from a one-mode photon subsystem, by choosing the generator $W_{\mathbf{k}}$ such that

$$
V_{\mathbf{k}} + [W_{\mathbf{k}}, H_{\mathbf{k};0}] = 0.
\tag{30}
$$

By substituting the solution of Eq. (30) into Eq. (29), one can obtain the standard form of the Schrieffer-Wolff Hamiltonian,

$$
H_{\mathbf{k}}' = H_{\mathbf{k};0} + \tfrac{1}{2}[W_{\mathbf{k}}, V_{\mathbf{k}}] + O(V_{\mathbf{k}}^3),
\tag{31}
$$

up to first order in the interaction term $V_{\mathbf{k}}$.

Equation (30) always has a definite solution as the perturbative component $V_{\mathbf{k}}$ is off-diagonal in the eigenbasis of $H_{\mathbf{k};0}$. By solving Eq. (30), we obtain the generator of the Schrieffer-Wolff transformation,

$$
W_{\mathbf{k}} = \left[\frac{g_{\text{m-ph}}^{\mathbf{k}}}{\omega_{\alpha_{\mathbf{k}}} - \omega_{c_{\mathbf{k}}}} c_{\mathbf{k}}^{\dagger}\alpha_{\mathbf{k}} - \frac{g_{\text{ph-q}}^{\mathbf{k}}}{\omega_q - \omega_{c_{\mathbf{k}}}} \eta^{\dagger}c_{\mathbf{k}} \right] - \text{H.c.},
\tag{32}
$$

which leads to the following block-diagonal hybrid Hamiltonian:

$$
\begin{aligned}
H_{\mathbf{k}}' &= H_{\mathbf{k};0} + \tfrac{1}{2}[W_{\mathbf{k}}, V_{\mathbf{k}}] \\
&= \omega_{c_{\mathbf{k}}}' c_{\mathbf{k}}^{\dagger}c_{\mathbf{k}} + \omega_{\alpha_{\mathbf{k}}}' \alpha_{\mathbf{k}}^{\dagger}\alpha_{\mathbf{k}} + \omega_q' \eta^{\dagger}\eta \\
&\quad + g_{\text{m-q}}^{\mathbf{k}} \eta^{\dagger}\alpha_{\mathbf{k}} + (g_{\text{m-q}}^{\mathbf{k}})^* \alpha_{\mathbf{k}}^{\dagger}\eta,
\end{aligned}
\tag{33}
$$

where

$$
\begin{aligned}
\omega_{c_{\mathbf{k}}}' &= \omega_{c_{\mathbf{k}}} - \frac{\left| g_{\text{m-ph}}^{\mathbf{k}} \right|^2}{\omega_{\alpha_{\mathbf{k}}} - \omega_{c_{\mathbf{k}}}} - \frac{\left| g_{\text{ph-q}}^{\mathbf{k}} \right|^2}{\omega_q - \omega_{c_{\mathbf{k}}}}, \\
\omega_{\alpha_{\mathbf{k}}}' &= \omega_{\alpha_{\mathbf{k}}} + \frac{\left| g_{\text{m-ph}}^{\mathbf{k}} \right|^2}{\omega_{\alpha_{\mathbf{k}}} - \omega_{c_{\mathbf{k}}}}, \\
\omega_q' &= \omega_q + \frac{\left| g_{\text{ph-q}}^{\mathbf{k}} \right|^2}{\omega_q - \omega_{c_{\mathbf{k}}}}, \\
g_{\text{m-q}}^{\mathbf{k}} &= g_{\text{m-ph}}^{\mathbf{k}} g_{\text{ph-q}}^{\mathbf{k}} \left[\frac{1}{\omega_{\alpha_{\mathbf{k}}} - \omega_{c_{\mathbf{k}}}} + \frac{1}{\omega_q - \omega_{c_{\mathbf{k}}}} \right].
\end{aligned}
\tag{34}
$$

As the photon mode is effectively decoupled from the rest of the Hamiltonian in Eq. (33), the effective magnon-transmon interacting Hamiltonian reads

$$
H_{\text{m-q}}^{\mathbf{k};\text{eff}} = \omega_{\alpha_{\mathbf{k}}}' \alpha_{\mathbf{k}}^{\dagger}\alpha_{\mathbf{k}} + \omega_q' \eta^{\dagger}\eta + g_{\text{m-q}}^{\mathbf{k}} \eta^{\dagger}\alpha_{\mathbf{k}} + (g_{\text{m-q}}^{\mathbf{k}})^* \alpha_{\mathbf{k}}^{\dagger}\eta.
\tag{35}
$$

We note that this effective magnon-transmon Hamiltonian looks similar to the one considered for a magnon in a ferromagnetic material [5–12]. However, in contrast to ferromagnetic materials where such hybridization is based on a Kittel magnon mode, for AFM materials, hybridization is based on the hybridized magnon mode α, which corresponds to the superposition of two Kittel modes a and b [see Eq. (3)]. Moreover, unlike in the ferromagnetic case where magnon-transmon hybridization is achieved with a linearly polarized microwave cavity field, the derivation of the AFM-based Hamiltonian in Eq. (35) requires a circularly polarized microwave cavity field [see the discussion below Eq. (18)]. Assuming a linearly polarized cavity mode would couple the qubit to both magnon modes α and β in the AFM system, thereby making it impossible to distinguish between different magnon modes and chiralities, as well as characterize magnon-magnon entanglement, which are among the main objectives of the analysis presented in this work.

B. Transmon qubit to probe magnons and their quantum characteristics in AFMs

The computational basis of the transmon qubit consists of the ground and first excited states $|0\rangle \equiv |g\rangle$ and $|1\rangle \equiv |e\rangle$, respectively, of the anharmonic oscillator in the transmon regime. In this case, the raising and lowering operators of the transmon qubit can be represented as $\eta^\dagger = |1\rangle\langle 0|$ and $\eta = |0\rangle\langle 1|$. The eigenstates of the number operator

$$N_{\mathbf{k}} = \alpha_{\mathbf{k}}^\dagger \alpha_{\mathbf{k}} + \eta^\dagger \eta = \alpha_{\mathbf{k}}^\dagger \alpha_{\mathbf{k}} + |1\rangle\langle 1| \qquad (36)$$

are $\{|0, 0\rangle; |1, 0\rangle, |0, 1\rangle; \cdots; |n, 0\rangle, |n - 1, 1\rangle; \cdots\}$, where the first entry counts the number of magnons in the hybridized mode α and the second entry labels the qubit state. These eigenstates span the magnon-qubit Hilbert space. The number operator commutes with the effective Hamiltonian in Eq. (35), i.e.,

$$[N_{\mathbf{k}}, H_{m-q}^{\mathbf{k};\text{eff}}] = 0. \qquad (37)$$

This implies that the effective Hamiltonian takes the block-diagonal form,

$$H_{m-q}^{\mathbf{k};\text{eff}} = \bigoplus_{n=0} H_{m-q}^{\mathbf{k};n}, \qquad (38)$$

where n is the eigenvalue of the number operator $N_{\mathbf{k}}$, i.e., counts the total number of magnon and transmon excitations. Except for the case $n = 0$ that the Hamiltonian submatrix is a one-dimensional block, for each $n > 0$ the block Hamiltonians $H_{m-q}^{\mathbf{k};n}$ are a 2×2 matrix of the form

$$H_{m-q}^{\mathbf{k};n} = \begin{pmatrix} n\omega_{\alpha_{\mathbf{k}}}' & \sqrt{n}\left(g_{m-q}^{\mathbf{k}}\right)^* \\ \sqrt{n}g_{m-q}^{\mathbf{k}} & n\omega_{\alpha_{\mathbf{k}}}' - 2\Delta_{\mathbf{k}} \end{pmatrix}, \qquad (39)$$

with $\Delta_{\mathbf{k}} = (\omega_{\alpha_{\mathbf{k}}}' - \omega_q')/2$ being the detuning between the magnon and qubit frequencies.

By shifting the qubit energy levels $|0\rangle$ and $|1\rangle$ with the amount of $\Delta_{\mathbf{k}}$, we may rewrite the Hamiltonian in Eq. (39) as an effective single transmon-qubit Hamiltonian,

$$H_q^{\text{eff}} = n\omega_{\alpha_{\mathbf{k}}}' \mathbb{I} + \sqrt{n}\Omega_{\mathbf{k}}^x \sigma_x + \sqrt{n}\Omega_{\mathbf{k}}^y \sigma_y + \Delta_{\mathbf{k}} \sigma_z, \qquad (40)$$

for each n. Here, $\Omega_{\mathbf{k}} = \Omega_{\mathbf{k}}^x + i\Omega_{\mathbf{k}}^y = g_{m-q}^{\mathbf{k}}$ characterizes the Rabi frequency of the qubit, $\mathbb{I}$ is the 2×2 identity matrix, and σ_l, $l = x, y, z$, are the Pauli matrices in the ordered effective qubit basis $\{|n, 0\rangle, |n - 1, 1\rangle\}$. This Hamiltonian results in the following energy eigensystem:

$$\epsilon_\pm = n\omega_{\alpha_{\mathbf{k}}}' \pm \sqrt{\Delta_{\mathbf{k}}^2 + n|\Omega_{\mathbf{k}}|^2},$$

$$|\epsilon_+\rangle = \cos\left(\frac{\theta_{\mathbf{k}}}{2}\right)|n, 0\rangle + e^{i\phi_{\mathbf{k}}}\sin\left(\frac{\theta_{\mathbf{k}}}{2}\right)|n - 1, 1\rangle,$$

$$|\epsilon_-\rangle = \sin\left(\frac{\theta_{\mathbf{k}}}{2}\right)|n, 0\rangle - e^{i\phi_{\mathbf{k}}}\cos\left(\frac{\theta_{\mathbf{k}}}{2}\right)|n - 1, 1\rangle, \qquad (41)$$

with $\Omega_{\mathbf{k}} = |\Omega_{\mathbf{k}}|e^{i\phi_{\mathbf{k}}}$ and $\tan\theta_{\mathbf{k}} = \frac{|\Omega_{\mathbf{k}}|}{\Delta_{\mathbf{k}}}$.

Suppose the transmon qubit is initialized in the state $|0\rangle$ at time $t = 0$ for a fixed n, for instance $n = 1$, that is $|\psi(0)\rangle = |1, 0\rangle$. Governed by the effective qubit Hamiltonian

in Eq. (40), the initial state evolves to

$$|\psi(t)\rangle = e^{-itH_q^{\text{eff}}}|\psi(0)\rangle$$

$$= e^{-it\epsilon_+}\cos\left(\frac{\theta_{\mathbf{k}}}{2}\right)|\epsilon_+\rangle + e^{-it\epsilon_-}\sin\left(\frac{\theta_{\mathbf{k}}}{2}\right)|\epsilon_-\rangle, \qquad (42)$$

after time t, which give rise to the following Rabi oscillation:

$$P_{0\to 1}(t) = |\langle 1|\psi(t)\rangle|^2 = \sin^2(\theta_{\mathbf{k}})\sin^2\left(\frac{(\epsilon_+ - \epsilon_-)t}{2}\right)$$

$$= \frac{|\Omega_{\mathbf{k}}|^2}{\Delta_{\mathbf{k}}^2 + |\Omega_{\mathbf{k}}|^2}\sin^2\left(\frac{(\epsilon_+ - \epsilon_-)t}{2}\right). \qquad (43)$$

This indicates that the probability of finding the transmon qubit in the state $|1\rangle$ after time t oscillates with the frequency

$$f_{\mathbf{k}} = (\epsilon_+ - \epsilon_-) = 2\sqrt{\Delta_{\mathbf{k}}^2 + |\Omega_{\mathbf{k}}|^2}, \qquad (44)$$

and intensity

$$I_{\mathbf{k}} = \frac{|\Omega_{\mathbf{k}}|^2}{\Delta_{\mathbf{k}}^2 + |\Omega_{\mathbf{k}}|^2}. \qquad (45)$$

Note that the maximum intensity $I_{\mathbf{k}} = 1$ occurs at the zero detuning $\Delta_{\mathbf{k}} = 0$, which is equivalent to the following qubit parameter tuning:

$$\omega_q = \omega_{\alpha_{\mathbf{k}}}, \qquad \left|g_{\text{ph-q}}^{\mathbf{k}}\right| = \left|g_{\text{m-ph}}^{\mathbf{k}}\right|. \qquad (46)$$

The detuning can be achieved, for instance, by appropriate adjustments of photon frequency and amplitude of the vector potential, as well as an applied magnetic field in the z direction, as depicted in Fig. 1. As a result of zero detuning, the angular frequency of the Rabi oscillation becomes

$$f_{\mathbf{k}} = \frac{4\left|g_{\text{m-ph}}^{\mathbf{k}}\right|^2}{|\omega_q - \omega_{c_{\mathbf{k}}}|} = \frac{4\lambda_{\mathbf{k}}^2}{|\omega_q - \omega_{c_{\mathbf{k}}}|}\Delta[\psi_{00}(r_{\mathbf{k}}, \phi_{\mathbf{k}})], \qquad (47)$$

where

$$\Delta[\psi_{00}(r_{\mathbf{k}}, \phi_{\mathbf{k}})] = \cosh 2r_{\mathbf{k}} + \sinh 2r_{\mathbf{k}}\cos\phi_{\mathbf{k}} \qquad (48)$$

is the the Einstein-Podolsky-Rosen (EPR) function for the two-mode ground state $|\psi_{00}(r_{\mathbf{k}}, \phi_{\mathbf{k}})\rangle$ given by Eq. (20) [21,22] (see the Appendix for details about EPR). The EPR function, which characterizes the Bell-type nonlocal correlations known as EPR nonlocality, is a highly relevant concept in the study of continuous variable entanglement [39,43].

We can always assume the parameter $\Gamma_{\mathbf{k}}$ in Eq. (4) to be real valued, in which case $\phi_{\mathbf{k}} = 0$ or π and thus

$$\Delta[\psi_{00}(r_{\mathbf{k}}, \phi_{\mathbf{k}})] = \begin{cases} e^{2r_{\mathbf{k}}} & \text{if} \quad \phi_{\mathbf{k}} = 0 \ (\Gamma_{\mathbf{k}} < 0) \\ e^{-2r_{\mathbf{k}}} & \text{if} \quad \phi_{\mathbf{k}} = \pi \ (\Gamma_{\mathbf{k}} > 0). \end{cases} \qquad (49)$$

Since the ground state EPR function and the magnon-magnon entanglement entropies all depend on the same entanglement (squeezing) parameter, one may observe the magnon-magnon entanglement through the EPR function $\Delta[\psi_{00}(r_{\mathbf{k}}, \phi_{\mathbf{k}})]$ and, in fact, through the qubit angular frequency in Eq. (47) of the Rabi oscillation. For instance, we obtain the entanglement entropy for the two-mode ground state,

$$E[|\psi_{00}(r_{\mathbf{k}}, \phi_{\mathbf{k}})\rangle] = [\cosh^2(r_{\mathbf{k}})\log_2\cosh^2(r_{\mathbf{k}})$$
$$- \sinh^2(r_{\mathbf{k}})\log_2\sinh^2(r_{\mathbf{k}})], \qquad (50)$$
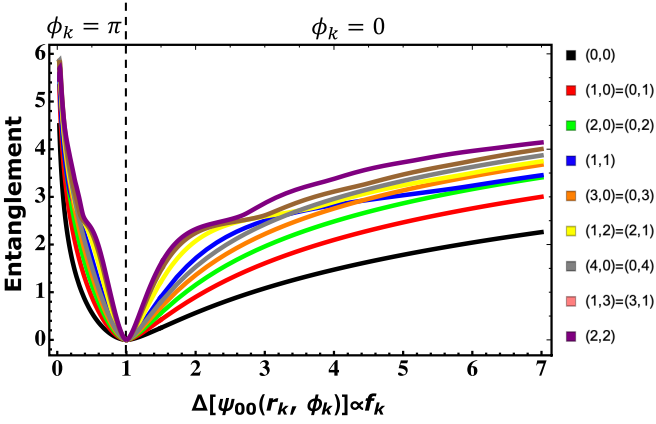
FIG. 5. Entanglement entropies of magnon eigenstates corresponding to selected pairs of magnon numbers (x, y) against the EPR function $\Delta[\psi_{00}(r_{\mathbf{k}}, \phi_{\mathbf{k}})]$ for AFM spin lattices. Stronger entanglement is observed for nonlocal states associated to $\phi_{\mathbf{k}} = \pi$, whereas $\phi_{\mathbf{k}} = 0$ represents a local state regime with weaker magnon-magnon entanglement.

as a function of the qubit angular frequency through

$$r_{\mathbf{k}} = \frac{e^{i\phi_{\mathbf{k}}}}{2} \Delta[\psi_{00}(r_{\mathbf{k}}, \phi_{\mathbf{k}})] = \frac{e^{i\phi_{\mathbf{k}}} |\omega_q - \omega_{c_{\mathbf{k}}}|}{8\lambda_{\mathbf{k}}^2} f_{\mathbf{k}}, \quad (51)$$

for $\phi_{\mathbf{k}} = 0, \; \pi$. Equation (51) follows from Eqs. (47) and (49). The entanglement entropies of all magnon eigenbasis states given by Eq. (26) are actually functions of the qubit angular frequency through the relation in Eq. (51). In practice, the entanglement entropy, given by Eq. (50), is a function of the parameter $r_{\mathbf{k}}$, which can be identified by Eq. (51) once the qubit angular frequency $f_{\mathbf{k}}$ has been determined experimentally. Figure 5 illustrates, as an example, the two-mode magnon entanglement in the ground (vacuum) state and number of excited states against the EPR function, $\Delta[\psi_{00}(r_{\mathbf{k}}, \phi_{\mathbf{k}})] \propto f_{\mathbf{k}}$, for AFM spin lattices.

Two distinct regions, i.e., the nonlocal bipartite entangled state $\phi_{\mathbf{k}} = \pi$ and the local bipartite entangled state $\phi_{\mathbf{k}} = 0$, with transition point at $\Delta[\psi_{00}(r_{\mathbf{k}}, \phi_{\mathbf{k}})] = 1$ can be distinguished in Fig. 5. The region of stronger magnon-magnon entanglement for a nonlocal two-mode magnon state is observed by the EPR uncertainty relation $\Delta[\psi_{00}(r_{\mathbf{k}}, \phi_{\mathbf{k}})] < 1$. The clear relation between the EPR function and the two-mode magnon entanglement entropy allows for experimental quantification of magnon-magnon entanglement through the EPR function $\Delta[\psi_{00}(r_{\mathbf{k}}, \phi_{\mathbf{k}})]$ and, indeed, the frequency $f_{\mathbf{k}}$ of Rabi oscillation of the transmon qubit. It is worth mentioning that the EPR nonlocality has been used for verification of entanglement in optical and atomic systems based on homodyne detection and types of interferometry setups [44–50]. However, these types of measurement setups are not realistic for magnon systems since these technologies are mainly based on beam splitters that have limitations for characterizing magnon entanglement. We propose, as a solution, a mechanism and measurement setup that rely on qubit-light-matter interaction as a probe to observe the EPR function, and thus EPR nonlocality and the degree of magnon-magnon entanglement. Moreover, Eq. (46) shows that at the zero detuning,
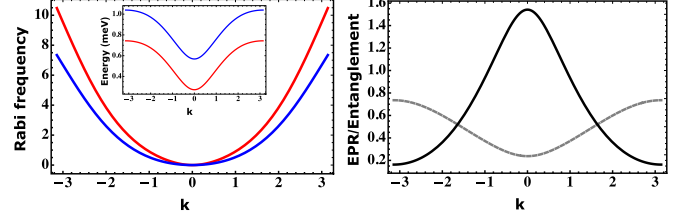

FIG. 6. Left panel: The angular frequency $f_{\mathbf{k}}$ of the Rabi oscillation of the transmon qubit depending on whether the transmon qubit is coupled to the magnon in α mode (red) through a right circularly polarized photon or to the magnon in β mode (blue) through a left circularly polarized photon. Inset: The corresponding dispersion energies for the two hybridized magnon modes α (red) and β (blue). Right panel: EPR function (gray dashed curve) and entanglement (black solid curve) between Kittel magnon modes in the vacuum ground state for different values of lattice momentum k. Similar results can be obtained for excited states. We assume uniaxial AFM materials [22] with a simple cubic lattice structure subjected to an external magnetic field in the z direction. The lattice momentum k takes its values along the $(0,0,1)$ direction with the lattice constant set to unity. We consider the nearest-neighbor Heisenberg interaction J and the easy-axis anisotropy $\mathcal{K}_z$ with model parameter values $J = 5$ meV, $\mathcal{K}_z = 0.01$ J, $B = 2$ T, for the amplitude of the magnetic field in the z direction, and $S = 1/2$. For the microwave cavity photon, we assume $A_0 = 1$ meV and $\omega_c = 0.05$ meV.

the magnon frequency in the hybridized α mode can also be observed through qubit frequency.

A similar procedure and formulation as above hold if we couple the transmon qubit to a bipartite AFM material instead through the magnon β mode, for instance, by using oppositely (left) circularly polarized light. Using different polarization for the photon would allow one to detect the twin chiral magnon modes in bipartite AFM materials. Figure 6 shows that the angular frequency $f_{\mathbf{k}}$ of the Rabi oscillation of a transmon qubit can observe and distinguish the two hybridized magnon modes in the system provided that appropriate polarized light is used. The figure also shows the correlation between indistinguishability of the two hybridized magnon modes, EPR nonlocality, and the entanglement between Kittel magnon modes. The higher the indistinguishability (around the zone center), the higher the nonlocality and entanglement.

We end the discussion with a remark on the parameter range relevant for experimental observation. Although the frequency of a transmon qubit depends on its physical design and operating conditions, transmon qubits typically operate at microwave frequencies, usually in the range of several to tens of gigahertz. Moreover, the frequency of a transmon qubit can be adjusted by modifying parameters such as the capacitance or the external magnetic field, making it a flexible and tunable system for quantum applications. On the other hand, magnons in AFM materials cover a wide range of frequencies that can be adjusted by certain parameters such as anisotropy and external magnetic field. Moreover gigahertz frequency antiferromagnetic materials, such as the antiferromagnetic insulator $CrCl_3$ [51], are available in nature. In Fig. 6 (inset), we plot the frequencies of magnons in a uniaxial AFM material, with some model parameter values provided in the caption of the figure. In such materials, magnons are typically in the

range of a few tens of gigahertz, which is the typical range of transmon-qubit frequencies. For larger and more tunable qubit frequencies, one may consider a flux-tunable transmon qubit in the proposed architecture shown in Fig. 1 [9]. Once the detuning condition in Eq. (46) is met, magnons, magnon chiralities, and magnon entanglement can be observed through the transmon Rabi frequency.

The discussion here has been based on a coupling between light and magnons coming from the B-field of the electromagnetic radiation. It is, of course, possible to also consider a coupling between magnons and light via the E-field, but in this case one has to consider multiferroic materials [52] with a well-documented coupling between electric field and magnetic degrees of freedom.

V. CONCLUSION

In conclusion, we demonstrate microwave cavity mediated hybridization of a superconducting transmon qubit and chiral magnons in bipartite AFM materials. We derive analytical expressions for the hybridized Hamiltonian and the coupling strengths. This coupling allows us not only to identify magnons in AFM materials, but also to verify their chirality and to characterize the nonlocality and bipartite entanglement between Kittel magnon modes in the system. These are all observed through measurement of the angular frequency of the Rabi oscillation in the transmon qubit. We hope the present work opens up a route to experimentally access rich quantum properties of magnons in AFM materials. The broad range of crystalline and synthetic AFM materials, such as the oxides NiO and MnO, the fluorides MnF_2 and FeF_2, 2D Ising systems such as $MnPSe_3$, the layered antiferromagnetic insulator $CrCl_3$, YIG-based synthetic AFMs, and perovskite manganites [13,26–33], provides a space for the experimental observation of the present results.

APPENDIX

Here, for a general two-mode quantum state $|\psi\rangle$, the EPR function is quantified by [39,43]

$$\Delta(\psi) = \tfrac{1}{2}\big[\mathrm{Var}_\psi\big(X_{\mathbf{k}}^A + X_{\mathbf{k}}^B\big) + \mathrm{Var}_\psi\big(P_{\mathbf{k}}^A - P_{\mathbf{k}}^B\big)\big], \quad \text{(A1)}$$

where $X_{\mathbf{k}}^A = \frac{a_{\mathbf{k}}+a_{\mathbf{k}}^\dagger}{\sqrt{2}}$ $\big(X_{\mathbf{k}}^B = \frac{b_{\mathbf{k}}+b_{\mathbf{k}}^\dagger}{\sqrt{2}}\big)$ and $P_{\mathbf{k}}^A = \frac{a_{\mathbf{k}}-a_{\mathbf{k}}^\dagger}{i\sqrt{2}}$ $\big(P_{\mathbf{k}}^B = \frac{b_{\mathbf{k}}-b_{\mathbf{k}}^\dagger}{i\sqrt{2}}\big)$ are assumed to be the dimensionless position and momentum quadratures for the $a_{\mathbf{k}}(b_{\mathbf{k}})$ mode, respectively. The $\mathrm{Var}_\psi(V)$ is the variance of an Hermitian operator V with respect to the state $|\psi\rangle$. The uncertainty relation $\Delta(\psi) \geqslant 1$ is known to hold for any given bipartite separable state $|\psi\rangle$ [43]. Therefore, any violation of this inequality is an indication of the state $|\psi\rangle$ being nonlocal and indeed a bipartite entangled state. Note that the EPR nonlocality specifies a stronger type of entanglement than a nonzero entropy of entanglement in the sense that there are states with nonzero entropy of entanglement which do not violate the uncertainty relation.

[1] A. Barman, G. Gubbiotti, S. Ladak, A. O. Adeyeye, M. Krawczyk, J. Gräfe, C. Adelmann, S. Cotofana, A. Naeemi, V. I. Vasyuchka, B. Hillebrands, S. A. Nikitov, H. Yu, D. Grundler, A. V. Sadovnikov, A. A. Grachev, S. E. Sheshukova, J.-Y. Duquesne, M. Marangolo, G. Csaba, W. Porod, V. E. Demidov, S. Urazhdin, S. O. Demokritov, E. Albisetti, D. Petti, R. Bertacco, H. Schultheiss, V. V. Kruglyak, V. D. Poimanov, S. Sahoo, J. Sinha, H. Yang, M. Münzenberg, T. Moriyama, S. Mizukami, P. Landeros, R. A. Gallardo, G. Carlotti, J.-V. Kim, R. L. Stamps, R. E. Camley, B. Rana, Y. Otani, W. Yu, T. Yu, G. E. W. Bauer, C. Back, G. S. Uhrig, O. V. Dobrovolskiy, B. Budinska, H. Qin, S. van Dijken, A. V. Chumak, A. Khitun, D. E. Nikonov, I. A. Young, B. W. Zingsem, and M. Winklhofer, The 2021 magnonics roadmap, J. Phys.: Condens. Matter **33**, 413001 (2021).

[2] H. Y. Yuan, Y. Cao, A. Kamra, R. A. Duine, P. Yan, Quantum magnonics: When magnon spintronics meets quantum information science, Phys. Rep. **965**, 1 (2022).

[3] D. D. Awschalom, C. H. R. Du, R. He, F. J. Heremans, A. Hoffmann, J. T. Hou, H. Kurebayashi, Y. Li, L. Liu, V. Novosad, J. Sklenar, S. E. Sullivan, D. Sun, H. Tang, V. Tiberkevich, C. Trevillian, A. W. Tsen, L. R. Weiss, W. Zhang, X. Zhang, L. Zhao, and C. W. Zollitsch, Quantum engineering with hybrid magnonics systems and materials, IEEE Trans. Quantum Eng. **2**, 1 (2021).

[4] Y. Li, W. Zhang, V. Tyberkevych, W.-K. Kwok, A. Hoffmann, and V. Novosad, Hybrid magnonics: Physics, circuits, and applications for coherent information processing, J. Appl. Phys. **128**, 130902 (2020).

[5] D. Lachance-Quirion, Y. Tabuchi, A. Gloppe, K. Usami, and Y. Nakamura, Hybrid quantum systems based on magnonics, Appl. Phys. Express **12**, 070101 (2019).

[6] A. A. Clerk, K. W. Lehnert, P. Bertet, J. R. Petta, and Y. Nakamura, Hybrid quantum systems with circuit quantum electrodynamics, Nat. Phys. **16**, 257 (2020).

[7] D. Lachance-Quirion, S. P. Wolski, Y. Tabuchi, S. Kono, K. Usami, and Y. Nakamura, Entanglement-based single-shot detection of a single magnon with a superconducting qubit, Science **367**, 425 (2020).

[8] Y. Tabuchi, S. Ishino, A. Noguchi, T. Ishikawa, R. Yamazaki, K. Usami, and Y. Nakamura, Quantum magnonics: The magnon meets the superconducting qubit, C. R. Phys. **17**, 729 (2016).

[9] S. Sharma, V. S. V. Bittencourt, and S. V. Kusminskiy, Protocol for generating an arbitrary quantum state of the magnetization in cavity magnonics, J. Phys. Mater. **5**, 034006 (2022).

[10] J.-K. Xie, S.-L. Ma, and F.-L. Li, Quantum-interference-enhanced magnon blockade in an yttrium-iron-garnet sphere coupled to superconducting circuits, Phys. Rev. A **101**, 042331 (2020).

[11] Y.-L. Ren, S.-L. Ma, and F.-L. Li, Chiral coupling between a ferromagnetic magnon and a superconducting qubit, Phys. Rev. A **106**, 053714 (2022).

[12] B. Z. Rameshti, S. V. Kusminskiy, J. A. Haigh, K. Usami, D. Lachance-Quirion, Y. Nakamura, C.-M. Hu, H. X. Tang, G. E. W. Bauer, and Y. M. Blanter, Cavity magnonics, Phys. Rep. **979**, 1 (2022).

[13] J. Li, S.-Y. Zhu and G. S. Agarwal, Magnon-Photon-Phonon Entanglement in Cavity Magnomechanics, Phys. Rev. Lett. **121**, 203601 (2018).

[14] J. Li and S.-Y. Zhu, Entangling two magnon modes via magnetostrictive interaction, New J. Phys. **21**, 085001 (2019).

[15] Z. Zhang, M. O. Scully, and G. S. Agarwal, Quantum entanglement between two magnon modes via Kerr nonlinearity driven far from equilibrium, Phys. Rev. Res. **1**, 023021 (2019).

[16] D. Bossini, S. Dal Conte, G. Cerullo, O. Gomonay, R. V. Pisarev, M. Borovsak, D. Mihailovic, J. Sinova, J. H. Mentink, T. Rasing, and A. V. Kimel, Laser-driven quantum magnonics and terahertz dynamics of the order parameter in so-called ferromagnets, Phys. Rev. B **100**, 024428 (2019).

[17] H. Y. Yuan, S. Zheng, Z. Ficek, Q. Y. He, and M.-H. Yung, Enhancement of magnon-magnon entanglement inside a cavity, Phys. Rev. B **101**, 014419 (2020).

[18] H. Y. Yuan, P. Yan, S. Zheng, Q. Y. He, K. Xia, and M.-H. Yung, Steady Bell State Generation via Magnon-Photon Coupling, Phys. Rev. Lett. **124**, 053602 (2020).

[19] Y. Tabuchi, S. Ishino, T. Ishikawa, R. Yamazaki, K. Usami, and Y. Nakamura, Hybridizing Ferromagnetic Magnons and Microwave Photons in the Quantum Limit, Phys. Rev. Lett. **113**, 083603 (2014).

[20] H. Y. Yuan and X. R. Wang, Magnon-photon coupling in so-called ferromagnets, Appl. Phys. Lett. **110**, 082403 (2017).

[21] V. Azimi-Mousolou, A. Bagrov, A. Bergman, A. Delin, O. Eriksson, Y. Liu, M. Pereiro, D. Thonig, and E. Sjöqvist, Hierarchy of magnon mode entanglement in antiferromagnets, Phys. Rev. B **102**, 224418 (2020).

[22] V. Azimi-Mousolou, Y. Liu, A. Bergman, A. Delin, O. Eriksson, M. Pereiro, D. Thonig, and E. Sjöqvist, Magnon-magnon entanglement and its quantification via a microwave cavity, Phys. Rev. B **104**, 224302 (2021).

[23] Y. Liu, A. Bagrov, A. Bergman, A. Delin, O. Eriksson, M. Pereiro, S. Streib, D. Thonig, E. Sjöqvist, and V. Azimi-Mousolou, Tunable and robust room-temperature magnon-magnon entanglement, arXiv:2209.01032.

[24] Y. Xiao, X. H. Yan, Y. Zhang, V. L. Grigoryan, C. M. Hu, H. Guo, and K. Xia, Magnon dark mode of an antiferromagnetic insulator in a microwave cavity, Phys. Rev. B **99**, 094407 (2019).

[25] Ø. Johansen and A. Brataas, Nonlocal Coupling between Antiferromagnets and Ferromagnets in Cavities, Phys. Rev. Lett. **121**, 087204 (2018).

[26] T. Kikkawa, K. Shen, B. Flebus, R. A. Duine, K. Uchida, Z. Qiu, G. E. W. Bauer, and E. Saitoh, Magnon Polarons in the Spin Seebeck Effect, Phys. Rev. Lett. **117**, 207203 (2016).

[27] H. T. Simensen, R. E. Troncoso, A. Kamra, and A. Brataas, Magnon-polarons in cubic collinear antiferromagnets, Phys. Rev. B **99**, 064421 (2019).

[28] T. T. Mai, K. F. Garrity, A. McCreary, J. Argo, J. R. Simpson, V. Doan-Nguyen, R. Valdés Aguilar, and A. R. HightWalker, Magnon-phonon hybridization in 2D antiferromagnet $MnPSe_3$, Sci. Adv. **7**, eabj3106 (2021).

[29] S. Liu, A. Granados del Águila, D. Bhowmick, C. Kwan Gan, T. Thu, Ha Do, M. A. Prosnikov, D. Sedmidubský, Z. Sofer, P. C. M. Christianen, P. Sengupta, and Q. Xiong, Direct Observation of Magnon-Phonon Strong Coupling in Two-Dimensional Antiferromagnet at High Magnetic Fields, Phys. Rev. Lett. **127**, 097401 (2021).

[30] C. Dai and F. Ma, Strong magnon-magnon coupling in synthetic antiferromagnets, Appl. Phys. Lett. **118**, 112405 (2021).

[31] E. G. Rini, M. N. Rao, S. L. Chaplot, N. K. Gaur, and R. K. Singh, Phonon dynamics of lanthanum manganite $LaMnO_3$ using an interatomic shell model potential, Phys. Rev. B **75**, 214301 (2007).

[32] H. Ulbrich, F. Krüger, A. A. Nugroho, D. Lamago, Y. Sidis, and M. Braden, Spin-wave excitations in the ferromagnetic metallic and in the charge-, orbital-, and spin-ordered states in $Nd_{1-x}Sr_xMnO_3$ with $x \approx 0.5$, Phys. Rev. B **84**, 094453 (2011).

[33] S. M. Rezende, A. Azevedo, and R. L. Rodríguez-Suárez, Introduction to antiferromagnetic magnons, J. Appl. Phys. **126**, 151101 (2019).

[34] L. M. Sandratskii and P. Buczek, Lifetimes and chirality of spin waves in antiferromagnetic and ferromagnetic FeRh from the perspective of time-dependent density functional theory, Phys. Rev. B **85**, 020406(R) (2012).

[35] Y. Nambu, J. Barker, Y. Okino, T. Kikkawa, Y. Shiomi, M. Enderle, T. Weber, B. Winn, M. Graves-Brook, J. M. Tranquada, T. Ziman, M. Fujita, G. E. W. Bauer, E. Saitoh, and K. Kakurai, Observation of Magnon Polarization, Phys. Rev. Lett. **125**, 027201 (2020).

[36] X. Zhang, A. Galda, X. Han, D. Jin, and V. M. Vinokur, Broadband Nonreciprocity Enabled by Strong Coupling of Magnons and Microwave Photons, Phys. Rev. Appl. **13**, 044039 (2020).

[37] K. Y. Bliokh and F. Nori, Characterizing optical chirality, Phys. Rev. A **83**, 021803(R) (2011).

[38] J. Koch, T. M. Yu, J. Gambetta, A. A. Houck, D. I. Schuster, J. Majer, A. Blais, M. H. Devoret, S. M. Girvin, and R. J. Schoelkopf, Charge-insensitive qubit design derived from the Cooper pair box, Phys. Rev. A **76**, 042319 (2007).

[39] G. Giedke, M. M. Wolf, O. Krüger, R. F. Werner, and J. I. Cirac, Entanglement of Formation for Symmetric Gaussian States, Phys. Rev. Lett. **91**, 107901 (2003).

[40] M. Shiranzaei, J. Fransson, and V. Azimi-Mousolou, Temperature-anisotropy conjugate magnon squeezing in antiferromagnets, arXiv:2304.07602.

[41] M. Nielsen and I. Chuang, *Quantum Information and Computation* (Cambridge University Press, Cambridge, 2000).

[42] J. R. Schrieffer and P. A. Wolff, Relation between the Anderson and Kondo Hamiltonians, Phys. Rev. **149**, 491 (1966).

[43] M. Fadel, L. Ares, A. Luis, and Q. He, Number-phase entanglement and Einstein-Podolsky-Rosen steering, Phys. Rev. A **101**, 052117 (2020).

[44] C. Gross, H. Strobel, E. Nicklas, T. Zibold, N. Bar-Gill, G. Kurizki, and M. K. Oberthaler, Atomic homodyne detection of continuous-variable entangled twin-atom states, Nature (London) **480**, 219 (2011).

[45] S. Armstrong, M. Wang, R. Y. Teh, Q. Gong, Q. He, J. Janousek, H.-A. Bachor, M. D. Reid, and P. K. Lam, Multipartite Einstein-Podolsky-Rosen steering and genuine tripartite entanglement with optical networks, Nat. Phys. **11**, 167 (2015).

[46] J. Peise, I. Kruse, K. Lange, B. Lücke, L. Pezzè, J. Arlt, W. Ertmer, K. Hammerer, L. Santos, A. Smerzi, and C. Klempt, Satisfying the Einstein-Podolsky-Rosen criterion with massive particles, Nat. Commun. **6**, 8984 (2015).

[47] J.-C. Lee, K.-K. Park, T.-M. Zhao, and Y.-H. Kim, Einstein-Podolsky-Rosen Entanglement of Narrow-Band Photons from Cold Atoms, Phys. Rev. Lett. **117**, 250501 (2016).

[48] P. Kunkel, M. Prüfer, H. Strobel, D. Linnemann, A. Frölian, T. Gasenzer, M. Gärttner, and M. K. Oberthaler, Spatially distributed multipartite entanglement enables EPR steering of atomic clouds, Science **360**, 413 (2018).

[49] M. Fadel, T. Zibold, B. Décamps, and P. Treutlein, Spatial entanglement patterns and Einstein-Podolsky-Rosen steering in Bose-Einstein condensates, Science **360**, 409 (2018).

[50] J. Li, Y. Liu, N. Huo, L. Cui, S. Feng, X. Li, and Z. Y. Ou, Measuring continuous-variable quantum entanglement with parametric-amplifier-assisted homodyne detection, Phys. Rev. A **101**, 053801 (2020).

[51] D. MacNeill, J. T. Hou, D. R. Klein, P. Zhang, P. J. Herrero, and L. Liu, Gigahertz Frequency Antiferromagnetic Resonance and Strong Magnon-Magnon Coupling in the Layered Crystal CrCl₃, Phys. Rev. Lett. **123**, 047204 (2019).

[52] N. A. Hill, Why are there so few magnetic ferroelectrics? J. Phys. Chem. B **104**, 6694 (2000).